Space-dependent perfusion coefficient estimation in a 2D bioheat transfer problem

Fermín S. V. Bazán [*] , Luciano Bedin[†] and Leonardo S. Borges [‡]

Abstract

In this work, a method for estimating the space-dependent perfusion coefficient parameter in a 2D bioheat transfer model is presented. In the method, the bioheat transfer model is transformed into a time-dependent semidiscrete system of ordinary differential equations involving perfusion coefficient values as parameters, and the estimation problem is solved through a nonlinear least squares technique. In particular, the bioheat problem is solved by the method of lines based on an highly accurate pseudospectral approach, and perfusion coefficient values are estimated by the regularized Gauss-Newton method coupled with a proper regularization parameter. The performance of the method on several test problems is illustrated numerically.

Keywords: Pennes equation; Chebyshev pseudospectral methods; non linear least squares problems; regularized Gauss-Newton method.

1 Introduction

Knowledge of temperature profiles and blood perfusion of living biological tissues is important for medical therapies such as temperature-based disease diagnostics, cryosurgery, infrared light therapy, cancer hyperthermia, and laser surgery, among others [12, 30]. Unfortunately, both quantities are nonlinearly related and thus, difficult to estimate empirically or numerically. The difficulty arises from several factors peculiar to living tissues, e.g., the complex anatomical structure of tissue, the blood flow in vessels, the heat exchange between the skin and its environment [6, 27, 17, 26], etc. To account for all above factors it is often assumed that heat transfer between tissue and blood occurs across the wall of capillaries, where blood velocity is very low [24, 37], with all perfusion information being concentrated in the so called blood perfusion coefficient. Blood perfusion is characterized as the local blood flow rate through the capillary network of the tissue. It plays an important role in physiological processes such as thermoregulation and inflammation. Hence, changes in blood perfusion indicate abnormal physiologic or pathologic condition of the tissue. Thus, estimation methods of blood perfusion are of paramount importance for medical disease diagnostics and therapeutic procedures.

[*]Department of Mathematics, Federal University of Santa Catarina, 88040-900, Florianópolis SC, Brazil, fermin@mtm.ufsc.br. The work of this author was supported by CNPq, Brazil, grant 477093/2011-6.

[†]Department of Mathematics, Federal University of Santa Catarina, 88040-900, Florianópolis SC, Brazil, luciano.bedin@ufsc.br. The work of this author was supported by CNPq, Brazil, grant 477093/2011-6.

[‡]Department of Mathematics, Federal University of Santa Catarina, 88040-900, Florianópolis SC, Brazil, l.s.borges@ufsc.br. The work of this author was supported by CNPq, Brazil, grant 455842/2014-0.

NOMENCLATURE

Symbol	Quantity
ρ, c, κ	density, specific heat and thermal conductivity of the tissue
w_b, c_b	mass flow rate of blood and specific heat of the blood
θ, θ_a	temperature of the tissue and arterial blood temperature
h_m, h_e	volumetric rate of metabolic heat generation and external heat
η, θ_∞	heat transfer coefficient and environmental temperature
θ_b, θ_0	skin surface temperature and initial temperature of the tissue
$g_0, \widehat{L}$	reference source of heating generation and length of perfused tissue
U, P_f	dimensionless temperature of tissue and blood perfusion coefficient
G, B	dimensionless source of heating generation and Biot number
U_∞	dimensionless difference between environmental and arterial temperatures
U_0	dimensionless difference between initial and arterial temperatures
D, I_n	Chebyshev differentiation matrix and identity matrix of order $n \times n$
$\overline{U}_j(t), \overline{H}(t)$	auxiliary vector valued functions
e_j	j-th canonical vector of appropriate dimension
$\overline{H}, V(t)$	auxiliary vector and vector of approximations to $\overline{U}(t)$
A	coefficient matrix of semidiscrete system of ODEs
$S(t)$	source term for semidiscrete system of ODEs
$\overline{P}_f$	diagonal matrix consisting of P_f evaluated on the mesh
$\overline{G}(t)$	vector valued function consisting of G evaluated on the mesh
$V_k, t_k, \Delta t$	approximate value to $V(t_k)$, time level and timestep
$F_1, \ldots, F_4$	coefficients of CPS-RK4 method
$\widetilde{U}^{t_k}, \mathcal{O}$	measured temperature and domain for bioheat transfer model
$L^2(\mathcal{O}),\ H^p(\mathcal{O})$	space of square integrable functions and Sobolev space
$\mathfrak{p}^*, \mathfrak{F}(P_f)$	stationary point of $\mathfrak{F}(P_f)$ and functional associated to the inverse problem
$\mathsf{U}(t)$	approximation values to the solution U
$\mathsf{A}(\mathbf{p})$	parameter dependent square matrix for the system of ODEs
$\mathbf{p}, \mathsf{S}(t)$	vector of unknown parameters and source term
$U_{\ell_i}^{t_k}(\mathbf{p}), \widetilde{U}_{\ell_i}^{t_k}$	exact and measured temperatures
$\mathbf{p}^*, F(\mathbf{p})$	stationary point of $F(\mathbf{p})$ and nonlinear least squares functional
$\mathbf{U}(\mathbf{p}), \widetilde{\mathbf{U}}$	vector of computed temperatures and vector of measured temperatures
δ	error norm between actual and measured temperatures
$\mathcal{K}, \mathbf{J}(\mathbf{p})$	compact subset of $\mathbb{R}^N$ and sensitivity matrix as a function of $\mathbf{p}$
$\mathsf{V}(\mathbf{p})(t), \mathsf{W}(t)$	auxiliary functions in semidiscrete system
$\overline{\mathsf{P}}_f$	diagonal matrix containing approximate values of P_j on the mesh
$\mathbf{p}_f$	vector containing approximate values of P_j on the mesh
$\mathbf{p}_\delta^k$	kth approximation produced by regularized Gauss-Newton method
$\widehat{\mathbf{U}}(\mathbf{p})$	linear model around $\mathbf{p}_\delta^k$ at iteration k of RGN
$\lambda_k, \mathbf{L}$	sequence of regularization parameters and regularization matrix
$\mathbf{p}_e, \mathcal{N}(\cdot), \xi$	a priori estimate of $\mathbf{p}_f$, Null space of $(\cdot)$ and scale factor for λ_k
$\breve{k}, \tau_d$	truncation index, noise-level factor
$\varsigma, \Phi^{(k)}$	scale factor for λ_k if δ is not available and fixed-point iteration function
$r_\lambda^k, \mathbf{n}$	residual $r_\lambda^k = [\mathbf{U}(\mathbf{p}_\delta^k) - \widetilde{\mathbf{U}}] + \mathbf{J}^k(\mathbf{p}_\lambda^{(k)} - \mathbf{p}_\delta^k)$ and Gaussian random vector
$\mathbf{L}_1(m), \mathbf{L}_2(m)$	first and second order 1D discrete differential operator
$\mathcal{L}_1(m), \mathcal{L}_2(m)$	first and second order 2D discrete differential operator
$\lambda^{(j)}$	fixed-point sequence to compute regularization parameter λ_k at stage k

NOMENCLATURE

Acronym	**Meaning**
RK4	Fourth order Runge-Kutta method
RGN	Regularized Gauss-Newton
CPS	Pseudospectral Collocation method
CPS-RK2	Second order predictor-corrector method
CPS-RK4	Fourth order Runge-Kutta method
ODE	Ordinary Differential Equation
PDE	Partial Differential Equation
DP	Discrepancy principle
FP	Fixed-point method
GSVD	Generalized singular value decomposition
RGN-FP	RGN algorithm coupled with FP
NL	Noise Level

The purpose of this investigation is to derive a method for the estimation of blood perfusion based on the combination of clinical temperature measurements with a mathematical model for heat transport proposed by Pennes [34] (referred to as the bioheat model) constrained to appropriate boundary conditions.

The 2D model is composed of a partial differential equation (PDE)

$$\rho c\, \theta_\tau - \kappa \Delta\theta + w_b c_b(\theta - \theta_a) = h_m + h_e, \quad 0 < x^* < \widehat{L},\ 0 < y^* < 1,\ \tau > 0, \tag{1}$$

and the boundary and initial conditions

$$\theta_{x^*} = 0, \quad x^* = 0,\ 0 < y^* < 1,\ \tau > 0, \tag{2}$$
$$\theta_{x^*} = 0, \quad x^* = \widehat{L},\ 0 < y^* < 1, \tau > 0, \tag{3}$$
$$\kappa\theta_{y^*} = \eta(\theta - \theta_\infty), \quad 0 < x^* < \widehat{L},\ y^* = 0,\ \tau > 0, \tag{4}$$
$$\theta = \theta_b, \quad 0 < x^* < \widehat{L},\ y^* = 1,\ \tau > 0, \tag{5}$$
$$\theta = \theta_0, \quad 0 < x^* < \widehat{L},\ 0 < y^* < 1,\ \tau = 0. \tag{6}$$

In this model, we consider a rectangular perfused tissue with length and thickness equal to $\widehat{L}$ and 1, respectively, see Fig. 1, and whose temperature at position (x^*, y^*) and time τ is denoted by $\theta(x^*, y^*, \tau)$. The parameters ρ, c and κ stand for density, specific heat and thermal conductivity of tissue, respectively. Moreover, h_e denotes the volumetric rate of external heat, h_m the volumetric rate of metabolic heat generation, θ_a the arterial temperature, c_b the specific heat of the blood and w_b the mass flow rate of blood per unit volume of tissue. The boundary conditions (2)-(5) include prescribed temperature on the upper skin surface at $y^* = 1$, adiabatic conditions at $x^* = 0$ and $x^* = \widehat{L}$, and convective heat transfer between the tissue and an adjoint large blood vessel at $y^* = 0$, as displayed in Fig. 1. Accordingly, η denotes the heat transfer coefficient, θ_∞ the environmental temperature (in the adjacent blood vessel) and θ_b the skin surface temperature; θ_0 is the initial temperature of the tissue.

Let us choose $g_0 > 0$ as a reference source of heating generation and suppose, for simplicity, that $\theta_a = \theta_b$. Letting

$$\begin{aligned} &U = \kappa g_0^{-1}\widehat{L}^{-2}(\theta - \theta_a),\ L = \widehat{L}^{-1},\ (x, y) = \widehat{L}^{-1}(x^*, y^*),\ t = \kappa\rho^{-1}c^{-1}\widehat{L}^{-2}\tau, \\ &P_f = w_b c_b \widehat{L}^2\kappa^{-1},\ B = \eta\widehat{L}\kappa^{-1},\ G = (h_e + h_m)g_0^{-1}, U_\infty = \kappa g_0^{-1}\widehat{L}^{-2}(\theta_\infty - \theta_a), \\ &U_0 = \kappa g_0^{-1}\widehat{L}^{-2}(\theta_0 - \theta_a), \end{aligned} \tag{7}$$

the dimensionless form of the system (1)-(6) reads

$$U_t - \Delta U + P_f U = G, \quad 0 < x < 1,\ 0 < y < L,\ t > 0, \tag{8}$$
$$U_x = 0, \quad x = 0,\ 0 < y < L,\ t > 0, \tag{9}$$
$$U_x = 0, \quad x = 1,\ 0 < y < L,\ t > 0, \tag{10}$$
$$U_y = B(U - U_\infty), \quad y = 0,\ 0 < x < 1,\ t > 0, \tag{11}$$
$$U = 0, \quad y = L,\ 0 < x < 1,\ t > 0, \tag{12}$$
$$U = U_0, \quad 0 < x < 1,\ 0 < y < L,\ t = 0. \tag{13}$$

The parameter P_f given above is the so called blood perfusion coefficient [34],[29], [28]; in turn, B corresponds to the well known Biot number [23], G is the dimensionless source of heating generation, U_∞ and U_0 stand by the dimensionless difference between the environmental and arterial temperatures and between the initial and the arterial temperatures, respectively.

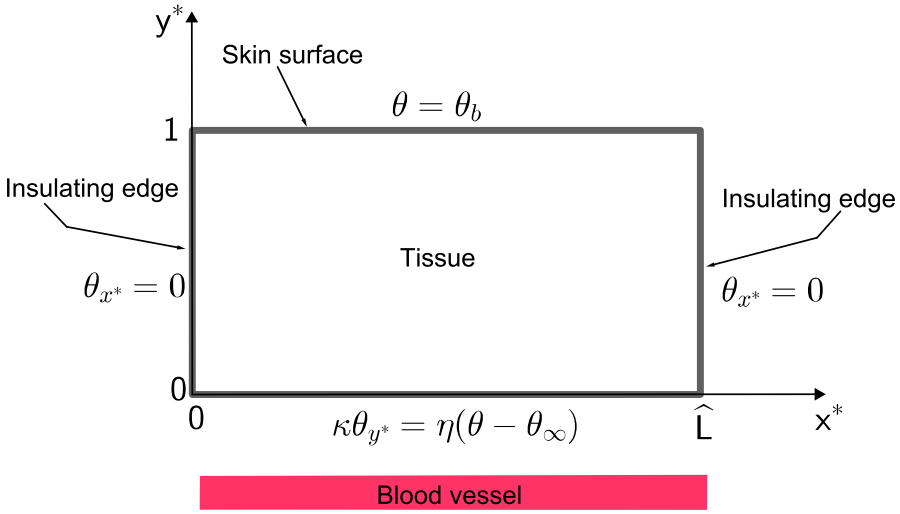

Figure 1: Domain for perfusion estimation.

Having described the bioheat transfer model, the estimation problem can be roughly described as follows: Given a set of measured temperature values $\widetilde{U}$ in prescribed locations, find a pair (P_f, U) satisfying the bioheat transfer model (1)-(6) such that U is close to $\widetilde{U}$ in some sense. A key element in the estimation procedure is to recognize that since the measurement data are indirectly correlated to the blood perfusion coefficient, the problem at hand is a nonlinear inverse and ill-posed parameter identification problem, where we are given a set of noisy temperature measurements and the perfusion coefficient (regarded as unknown) needs to be estimated through nonlinear techniques [11, 31, 25, 28]. As a matter of fact, we note that in real life, the perfusion coefficient is a dimensionless clinical parameter that changes with the evolution of temperature due to the very complex nature of the pathways through which it flows [15, 24]. For these complications, the perfusion coefficient is often regarded as a function that depends on time and position and not on temperature field [41, 42]. In this investigation we restrict ourselves to the case where the perfusion coefficient does not depend on time.

Inverse blood perfusion estimation techniques for one dimensional cases based on known initial and Dirichlet boundary conditions and additional heat flux measurements have been described by Trucu et al. [41, 42]; a procedure based on integral transform techniques in rectangular domains is addressed in [29], while the boundary element method is employed in [22, 33]. A more general model including porosity effects is introduced in [6]; in [15] are described estimates for temperature dependent blood perfusion in complex 3D domains. In our approach, the bioheat transfer model (8)-(13) (the forward problem) is transformed into a time-dependent semidiscrete system of ordinary differential equations involving perfusion coefficient values as

a set of unknown parameters, and the parameter estimation problem (i.e., the determination of estimates for all parameters) is solved through a nonlinear least squares technique. More precisely, the forward problem is solved by the method of lines, based on an accurate pseudospectral approach to perform the spatial discretization of the PDE defined in (8) together with two time integrator methods, namely a second order predictor-corrector method and the fourth order Runge-Kutta method. Perfusion coefficient values are then estimated by a nonlinear minimization protocol based on the regularized Gauss-Newton method (RGN) [41] in conjunction with the Fixed-point method (FP) [2, 3, 4, 5] as regularization parameter choice rule. The approach requires the solution of the forward problem at each iteration with estimates of P_f as input data.

The paper is organized as follows. A detailed discretization procedure of the direct problem and some numerical results are presented in Section 2. In Section 3 the inverse problem is discussed and the non linear protocol is established. In section 4 we present some numerical results that illustrate the performance of the method on several synthetic test problems. The paper ends with final considerations.

2 Forward Problem

In previous investigations, analytical and numerical aspects of the bioheat equation have been considered in applications that include hyperthermic treatment, cryosurgery, thermoregulation analysis and others. For example, analytical solutions for the 1D Pennes equation based on fundamental solutions for parabolic equations were presented in [1] and [20]; oscillatory heat flux condition with the aid of Laplace transform method has been considered in [37]; in [13] the authors deal with transient coefficients by spectral element methods, while in [1], concentric spherical regions are addressed by the finite difference method (see also [36]). Solutions for a 2D bioheat equation involving convective boundary conditions based on integral transform techniques are described in [29], and more recently, a pseudospectral approach is proposed in [8]; in [12] a Monte Carlo method was developed to solve a 3D Pennes equation with nonlinear boundary conditions. A rigorous mathematical analysis concerning existence and uniqueness of solution to the model (8)-(13), in Sobolev space settings, can be found in [7, Theorem 3.1], in which, the solution U is expressed in Fourier series form in terms of eigenfunctions of the elliptic operator $-\Delta + P_f I$. However, such solution is difficult to compute in practice.

In this section, as an alternative to existing numerical approaches in literature, we will consider a numerical method for the bioheat problem (8)-(13) based on the well known pseudospectral collocation (CPS) method. The CPS approach has become an efficient way to construct approximate solutions to partial differential equations (PDEs), see, e.g., [8, 18, 40], due to its high precision and relatively lower computation cost compared to finite difference methods. It has also been proven successful in solving a stationary 2D forward problem associated to an inverse heat flux estimation problem in coiled tubes [9]. In the present case, the underlying idea is to approximate spatial derivatives by using the differentiation Chebyshev matrix, which gives rise to a system of ordinary differential equations (ODEs) where only the time derivative appears, and then integrate in time by some appropriate numerical scheme for ODEs. For simplicity we shall consider a mesh consisting of $(n+1)\times(n+1)$ grid points on the unit square based on $(n+1)$ Chebyshev-Gauss Lobatto points in each direction:

$$x_i = \frac{1}{2}\left(1-\cos\frac{\pi i}{n}\right), \quad 0\le i\le n, \quad y_j = \frac{1}{2}\left(1-\cos\frac{\pi j}{n}\right), \quad 0\le j\le n, \tag{14}$$

and assume that the grid points are numbered in the lexicographic ordering, as seen in Fig. 2.

Let the $(n+1)\times(n+1)$ differentiation Chebyshev matrix in $[0,1]$ be denoted by D and

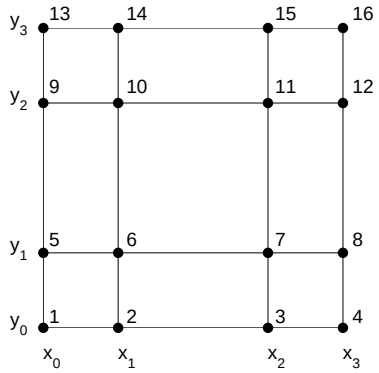

Figure 2: Grid comprising 16 points corresponding to $n = 3$.

assume that it can be described in column-wise (resp. row-wise) form as

$$D = [d_0\ d_1\ \cdots\ d_n] = \begin{bmatrix} r_0^T \\ \vdots \\ r_n^T \end{bmatrix}, \quad d_i, r_i \in \mathbb{R}^{n+1}. \tag{15}$$

For later use define

$$D_1 = [d_1\ d_2\ \cdots d_{n-1}], \quad D_2 = \begin{bmatrix} r_1^T \\ \vdots \\ r_{n-1}^T \end{bmatrix}, \tag{16}$$

$$\overline{U}_j(t) = [U(x_0, y_j, t),\ U(x_1, y_j, t),\ \cdots U(x_n, y_j, t)]^T,\ 0 \le j \le n. \tag{17}$$

To approximate second order derivatives with respect to x notice that the second order Chebyshev differentiation matrix, D^2, can be expressed as

$$D^2 = d_0 r_0^T + d_1 r_1^T + \cdots + d_n r_n^T. \tag{18}$$

Therefore

$$\begin{aligned} \begin{bmatrix} U_{xx}(x_0, y_j, t) \\ U_{xx}(x_1, y_j, t) \\ \vdots \\ U_{xx}(x_n, y_j, t) \end{bmatrix} &\approx D^2 \begin{bmatrix} U(x_0, y_j, t) \\ U(x_1, y_j, t) \\ \vdots \\ U(x_n, y_j, t) \end{bmatrix} = d_0 r_0^T \overline{U}_j(t) + D_1 D_2 \overline{U}_j(t) + d_n r_n^T \overline{U}_j(t) \\ &\approx D_1 D_2 \overline{U}_j(t), \qquad 0 \le j \le n-1, \end{aligned} \tag{19}$$

where we have used the fact that $r_i^T \overline{U}_j \approx U_x(x_i, y_j, t)$, the boundary conditions (9)-(10), and the definitions in (16). Therefore, taking the ordering of the grid points into account, we can consider the vector of all unknown on the mesh :

$$\overline{U}(t) = [\overline{U}_0(t)^T\ \overline{U}_1(t)^T\ \cdots \overline{U}_{n-1}(t)^T]^T,$$

and use (19) to obtain

$$\begin{bmatrix} U_{xx}(x_0, y_0, t) \\ \vdots \\ U_{xx}(x_n, y_0, t) \\ \vdots \\ U_{xx}(x_0, y_{n-1}, t) \\ \vdots \\ U_{xx}(x_n, y_{n-1}, t) \end{bmatrix} \approx (I_n \otimes D_1 D_2)\, \overline{U}(t) \tag{20}$$

where $\otimes$ stands for Kronecker product. This completes the approximation of second order derivatives with respect to x. A similar procedure shows that second order derivatives with respect to y can be approximated as

$$\begin{bmatrix} U_{yy}(x_0,y_0,t) \\ \vdots \\ U_{yy}(x_n,y_0,t) \\ \vdots \\ U_{yy}(x_0,y_{n-1},t) \\ \vdots \\ U_{yy}(x_n,y_{n-1},t) \end{bmatrix} \approx \left[\left(B\overline{d}_0 e_1^T + \overline{D}_1\overline{D}_2\right)\otimes I_{(n+1)}\right]\overline{U}(t) - B\,U_\infty\overline{H}, \tag{21}$$

where

$$\overline{D}_1 = [\overline{d}_1 \ldots \overline{d}_n], \quad \overline{D}_2 = \begin{bmatrix} \overline{r}_1^T \\ \vdots \\ \overline{r}_n^T \end{bmatrix} \tag{22}$$

with $\overline{d}_i$ and $\overline{r}_i$ being the vectors obtained by taking the first n components of d_i and r_i, $\overline{H} = [H_0^T, \ldots, H_{n-1}^T]^T$, with $H_i = e_{i+1}^T\overline{d}_0\,[1,\ldots,1]^T \in \mathbb{R}^{n+1}, \quad i = 0,\ldots,n-1$. This completes the discretization of spatial derivatives in the mesh.

Finally, neglecting discretization errors and denoting the vector of approximations to $\overline{U}(t)$ by $V(t)$, combination of (20), (21) and (8) yields an initial-value problem for a system of linear ordinary differential equations of the form

$$\begin{cases} V'(t) = AV(t) + S(t),\ t > 0 \\ V(0) = U_0, \end{cases} \tag{23}$$

where

$$A = \left[(I_n \otimes D_1D_2) + (B\overline{d}_0 e_1^T + \overline{D}_1\overline{D}_2)\otimes I_{(n+1)} - \overline{P}_f\right], \tag{24}$$

$$\overline{P}_f = \operatorname{diag}\left(P_f(x_0,y_0),\ldots,P_f(x_n,y_0),\ldots,P_f(x_0,y_{n-1}),\ldots,P_f(x_n,y_{n-1})\right), \tag{25}$$

and

$$S(t) = \overline{G}(t) - BU_\infty\overline{H}, \quad \text{with} \tag{26}$$

$$\overline{G}(t) = [G(x_0,y_0,t),\ldots,G(x_n,y_0,t),\ldots,G(x_0,y_{n-1},t),\ldots,G(x_n,y_{n-1},t)]^T. \tag{27}$$

Therefore, highly accurate approximate solution to model (1)-(6) can be computed by solving the initial-value problem (23). Notice that the solution to this initial-value problem can be computed using eigenvalues and eigenvectors of A using the fact that

$$V(t) = e^{At}V(0) + \int_0^t e^{A(t-\tau)}S(\tau)d\tau. \tag{28}$$

The capability of the CPS method to produce highly accurate numerical solutions relies on the fact that accurate approximation to the most important features of the PDE, namely the eigenvalues and corresponding eigenmodes, are now concentrated in the eigensystem of matrix A. For illustration we consider the case $P_f = cte$ (for which eigenpairs of the continuous problem are determined in closed form) and compute the first 100 eigenvalues of the continuous problem as well as their approximations obtained from matrix A for $n = 30$, see Figure 3.

To illustrate something similar with regard to eigenmodes, the first four continuous eigenmodes and the first four discrete eigenmodes are all displayed in Figure 4. Note that for $n = 30$, three of the continuous eigenmodes are already captured.

Summarizing, the CPS-based numerical approach for computing approximate solutions to the initial and boundary value problem involving the bioheat equation reduces to apply time

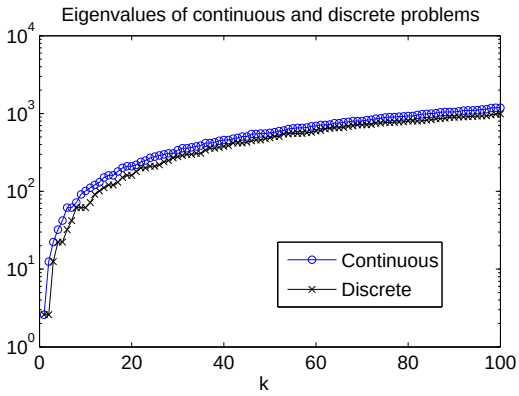

Figure 3: Eigenvalues of continuous and discrete problems for the data set described in (32).

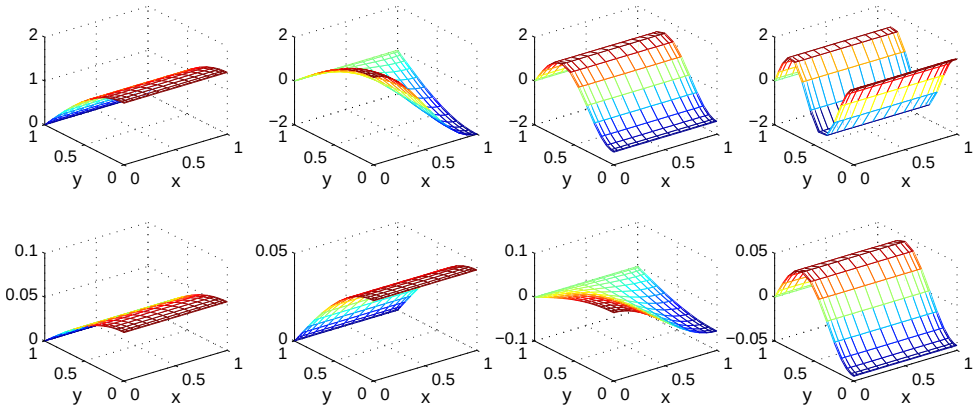

Figure 4: First four eigenmodes of continuous (top) and discrete (bottom) Bioheat problems.

integration methods for ODEs, like multi-step or Runge-Kutta methods, for solving the initial value problem (23). In our computations we consider two time integration methods, namely, a second order predictor-corrector method and the well-known fourth order Runge-Kutta method. The former, denoted here by **CPS-RK2**, combines the forward Euler method as a predictor and the Crank-Nicolson (also referred to as trapezoidal rule) as a corrector. If we let V_k denote the value that approximates $V(t_k)$, $t_k = \Delta t\, k$, **CPS-RK2** can be outlined as follows:

CPS-RK2:
For $k \geq 0$, calculate

$$\begin{aligned} V_{k+1}^{(p)} &= V_k + \Delta t\,(AV_k + S(t_k)) \\ V_{k+1} &= V_k + \frac{\Delta t}{2}\left[A\left(V_k + V_{k+1}^{(p)}\right) + S(t_k) + S(t_{k+1})\right]. \end{aligned} \tag{29}$$

The fourth order Runge-Kutta method, denoted by **CPS-RK4**, can be outlined as follows:

CPS-RK4:
For $k \geq 0$, calculate

$$V_{k+1} = V_k + \frac{\Delta t}{6}(F_1 + 2F_2 + 2F_3 + F_4), \qquad \text{with} \tag{30}$$

$$F_1 = AV_k + S(t_k), \quad F_2 = A\left(V_k + \frac{\Delta t}{2}F_1\right) + S(t_k + \frac{\Delta t}{2})$$
$$F_3 = A\left(V_k + \frac{\Delta t}{2}F_2\right) + S(t_k + \frac{\Delta t}{2}), \quad F_4 = A\left(V_k + \Delta t F_3\right) + S(t_{k+1}).$$

2.1 Numerical examples

We shall illustrate the effectiveness of the chosen time integration methods with two examples. The first example considers the perfusion coefficient constant case where the source term is taken to be

$$\begin{aligned} G(x,y,t) &= e^{at}y^2(y-L)\cos(\pi x)[a\cos(ct) - c\sin(ct)] \\ &\quad - e^{at}\cos(ct)\cos(\pi x)[-\pi^2 y^2(y-L) + (6y-2L)] - \frac{2BU_\infty}{L} \\ &\quad + P_f[e^{at}\cos(ct)y^2(y-L)\cos(\pi x) + \frac{BU_\infty}{L}y(y-L)] \end{aligned}$$

where a, c are arbitrary real constants, and the solution for the bioheat problem is

$$U(x,y,t) = e^{at}\cos(ct)y^2(y-L)\cos(\pi x) + \frac{BU_\infty}{L}y(y-L). \tag{31}$$

We report results obtained with **CPS-RK4** corresponding to the data

$$a = -50, \quad c = 3\pi, \quad B = 0.015, \quad P_f = 0.1, \quad L = 1, \quad \text{and} \quad U_\infty = 0.001, \tag{32}$$

for $n = 20$, which implies a grid of 21×21 points and a system matrix A of size 420×420. For this example the timestep is $\Delta t = 0.00004$, a slightly smaller value than the maximum allowable timestep for stable integration, the same timestep being used in the implementation of **CPS-RK2**. The results displayed in Figure 5 confirm what is known from literature: exponential accuracy for infinitely differentiable functions with regard to spatial variables and $\mathcal{O}(\Delta t)^4 \approx \mathcal{O}(10^{-16})$ accurate results for **RK4** as time integrator. For details concerning theoretical upper bounds for the error associated to spectral methods, the reader is referred to [10, 35]. The results obtained with **CPS-RK2** reached an accuracy of eight significant digits and were thus indistinguishable when compared with those obtained by **CPS-RK4**; these results are not reported here.

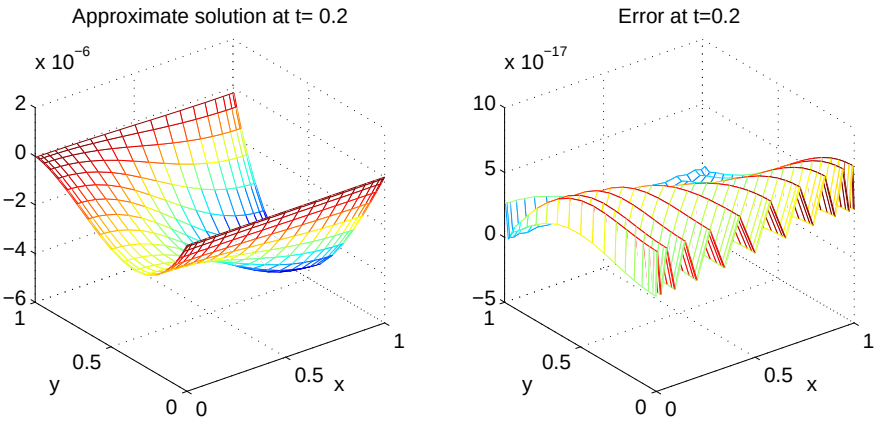

Figure 5: Approximate solution computed by **CPS-RK4** and corresponding error with respect to the exact solution in a grid of 21×21 points.

Our second example considers a bioheat problem where the perfusion coefficient is a non smooth function of x and the source term $G(x,y,t)$ is chosen in such a way that the solution $U(x,y,t)$ is the function defined in (31), where a, c, B, L and U_∞ are the same as in (32). In this case the perfusion coefficient is defined by

$$P_f(x) = \begin{cases} 0, & 0 \le x \le 0.2, \\ 10(x-0.2)/3, & 0.2 \le x \le 0.5, \\ -10(x-0.8)/3, & 0.5 \le x \le 0.8, \\ 0, & 0.8 \le x \le 1. \end{cases} \tag{33}$$

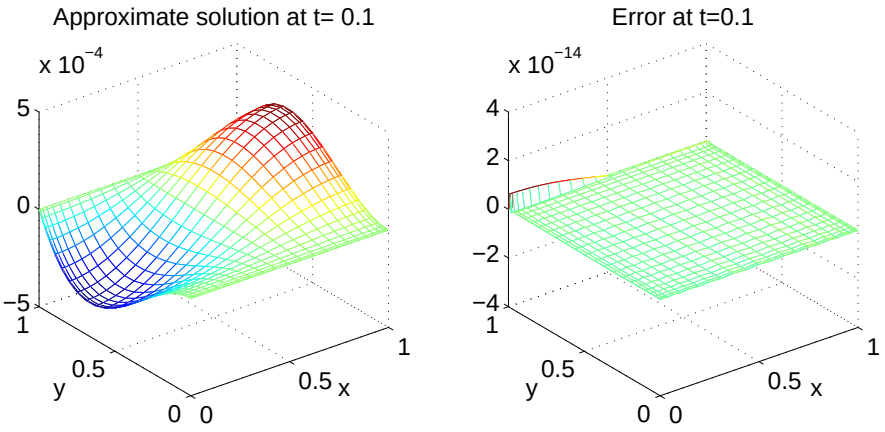

Figure 6: Numerical results for spatial-dependent perfusion coefficient case.

The results obtained with **CPS-RK4** for the case where $n = 20$ are displayed in Figure 6. We also emphasize that P_f given in (33) does not represent a realistic situation [29]; it is chosen simply to check the potential of the proposed numerical method.

3 Inverse problem of perfusion coefficient estimation: pseudospectral approach

Given that a numerically robust method for solving the bioheat model is available, we shall now introduce a numerical method for the associated inverse problem consisting of estimating the perfusion coefficient based on a set of measured temperatures as input data. Before this, we emphasize that although our main goal is not to treat the theoretical properties of this inverse problem, we find instructive to outline the question on existence of a solution as follows. Suppose that we are given measured temperatures $\widetilde{U}^{t_k} \in L^2(\mathcal{O})$, $\mathcal{O} =]0,1[\times]0,L[\times[0,T]$, at time levels $0 < t_1 < t_2 < \ldots < t_q < T$. Then the inverse problem consists in recovering (P_f, U) such that (8)-(13) is satisfied for $t \in [0,T]$ and $U(\cdot,t_k) = \widetilde{U}(\cdot,t_k)$, and can be reformulated as an optimization problem: Find $\mathfrak{p}^*$ defined as

$$\mathfrak{p}^* = \underset{P_f \in \mathcal{X}}{\operatorname{argmin}}\, \mathfrak{F}(P_f), \quad \mathfrak{F}(P_f) = \frac{1}{2}\sum_{k=1}^{q}\int_0^1\int_0^L \left(U(x,y,t_k) - \widetilde{U}^{t_k}(x,y)\right)^2 dydx, \tag{34}$$

where $\mathcal{X} = \{\mathfrak{p} \in L^2(\mathcal{O}),\ 0 \le \mathfrak{p} \le K,\ K > 0,\ \text{a. e. in } \mathcal{O}\}$, where $U \in C([0,T];L^2(\mathcal{O})) \cap C^1(]0,T];H^2(\mathcal{O}))$ is the solution of (8)-(13) corresponding to P_f. The existence of $\mathfrak{p}^* \in \mathcal{X}$ satisfying (34) can be proved using weak convergence arguments, compactness principles and [7, Theorem 3.1]. The details are beyond the scope of the paper.

The estimation approach proposed in this paper assumes that the initial-boundary value problem (8)-(13) is transformed into a system of ordinary differential equations (ODEs) in which only the time derivative appears. This means that discretization is made only in space, e.g., by means of finite differences, finite elements, spectral methods, etc, and that, due to the nature of the original problem, the discretization procedure gives rise to a system of ODEs of the form

$$\begin{cases} \mathsf{U}'(t) = \mathsf{A}(\mathbf{p})\mathsf{U}(t) + \mathsf{S}(t), \quad t > 0 \\ \mathsf{U}(0) = U_0, \end{cases} \tag{35}$$

where $\mathbf{p}$ is a vector of unknown parameters, $\mathsf{A}(\mathbf{p})$ is a square matrix that depends on $\mathbf{p}$ and the chosen discretization method, and the source term $\mathsf{S}(t)$ is a vector valued function that also depends on the chosen spatial discretization method. The solution of (35) is a vector valued

function that depends on $\mathbf{p}$ and contains approximations to the solution $U(x_i, y_j, t)$ of the bioheat problem (1)-(6) on the spatial grid; this solution is denoted by $\mathsf{U}(\mathbf{p}, t)$. For simplicity, for appropriate positive integers N, s, in what follows we assume that $\mathsf{A} : \mathbb{R}^N \to \mathbb{R}^s \times \mathbb{R}^s$ and $\mathsf{S} : [0, +\infty[\mapsto \mathbb{R}^s$ are sufficiently smooth maps. In such a case, for given $\mathbf{p} \in \mathbb{R}^N$ and $U_0 \in \mathbb{R}^s$, existence and uniqueness of $\mathsf{U}(\mathbf{p}, .)$ satisfying (35) is standard. Smooth dependence of parameters in linear ODE's systems (see [38, Section 6.2]) ensure smoothness of U in both variables t and $\mathbf{p}$. In particular, $\dfrac{\partial \mathsf{U}(\mathbf{p}, t)}{\partial p_j}$ is well defined for each $j = 1, \ldots, N$ and all $t \geq 0$.

Thus, the inverse problem of estimating the perfusion coefficient can be formulated as one of estimating a vector $\mathbf{p}$ of parameters such that the difference between computed temperatures $\mathsf{U}(\mathbf{p}, t)$ at prescribed locations and experimentally acquired temperatures at the same locations is minimized in some sense. For future reference, computed and experimentally measured temperatures at locations ℓ_i, $i = 1, 2, \ldots, M$, and time levels t_k, $k = 1, \ldots, q$, are denoted by $U_{\ell_i}^{t_k}(\mathbf{p})$ and $\widetilde{U}_{\ell_i}^{t_k}$, respectively. Moreover, measured temperatures are assumed to be corrupted by additive noise, that is

$$\widetilde{U}_{\ell_i}^{t_k} = U_{\ell_i}^{t_k} + \epsilon_i{}^k, \quad i = 1, \ldots, M, \ k =, \ldots, q \tag{36}$$

where ϵ_i^k are random numbers and $U_{\ell_i}^{t_k}$ are actual (exact) temperature values. Thus the perfusion estimation problem can be, in principle, handled by solving a non linear least squares problem of the form

$$\mathbf{p}^* = \underset{\mathbf{p} \in \mathbb{R}^N}{\operatorname{argmin}} \, F(\mathbf{p}), \quad F(\mathbf{p}) = \frac{1}{2} \|\mathbf{U}(\mathbf{p}) - \widetilde{\mathbf{U}}\|_2^2 = \frac{1}{2} \sum_{k=1}^{q} \sum_{i=1}^{M} (U_{\ell_i}^{t_k}(\mathbf{p}) - \widetilde{U}_{\ell_i}^{t_k})^2, \tag{37}$$

where $\mathbf{p} = [p_1, \ldots, p_N]^T$ is the vector of unknowns,

$$\mathbf{U}(\mathbf{p}) = [U_{\ell_1}^{t_1}(\mathbf{p}), \ldots, U_{\ell_M}^{t_1}(\mathbf{p}), U_{\ell_1}^{t_2}(\mathbf{p}), \ldots, U_{\ell_M}^{t_2}(\mathbf{p}), \ldots, U_{\ell_1}^{t_q}(\mathbf{p}), \ldots, U_{\ell_M}^{t_q}(\mathbf{p})]^T$$

is the vector of computed temperatures from model problem (35), and

$$\widetilde{\mathbf{U}} = [\widetilde{U}_{\ell_1}^{t_1}, \ldots, \widetilde{U}_{\ell_M}^{t_1}, \widetilde{U}_{\ell_1}^{t_2}, \ldots, \widetilde{U}_{\ell_M}^{t_2}, \ldots, \widetilde{U}_{\ell_1}^{t_q}, \ldots, \widetilde{U}_{\ell_M}^{t_q}]^T$$

is the vector of measured temperatures such that

$$\|\mathbf{U} - \widetilde{\mathbf{U}}\|_2 \leq \delta, \tag{38}$$

where $\mathbf{U}$ is the vector of actual (and exact) temperatures at location ℓ_i and time level t_k, and δ is an estimate of the error norm between actual and measured temperatures.

Notice from the continuity of U in $\mathbb{R}^N \times [0, +\infty[$ that the functional F is continuous on $\mathbb{R}^N$. Consequently, if we restrict $\mathbf{p}$ to a nonempty compact subset $\mathcal{K}$ of $\mathbb{R}^N$, F has a minimum at some $\mathbf{p}^* \in \mathcal{K}$. Hence, a reasonable choice is $\mathcal{K} = \{\mathbf{p} \in \mathbb{R}^N; \ 0 \leq p_j \leq K, \ j = 1, \ldots, N\}$ for chosen K, and the minimization problem can be addressed in a number of ways such as trust region methods or nonmonotone line search approaches [19, 39]. However, the existence of multiple minima can not be ruled out and therefore difficulties can always appear. Thus, methods that produce approximate minimizers preserving properties of the sought parameter are always desirable. The study and application of a method with these characteristics in the problem of estimating the perfusion coefficient is one of the main objectives of this work. We start this study with the observation that differentiation of F with respect to p_j gives

$$\frac{\partial F(\mathbf{p})}{\partial p_j} = \sum_{k=1}^{q} \sum_{\ell=1}^{M} (\widetilde{U}_{\ell_i}^{t_k}(\mathbf{p}) - \widetilde{U}_{\ell_i}^{t_k}) \frac{\partial U_{\ell_i}^{t_k}(\mathbf{p})}{\partial p_j}.$$

Hence a necessary condition for $\mathbf{p}^*$ to be a critical point of F,

$$\frac{\partial F(\mathbf{p}^*)}{\partial p_j} = 0, \quad j = 1, 2, \ldots, N,$$

can be rewritten in matrix form as

$$\mathbf{J}(\mathbf{p}^*)^T[\mathbf{U}(\mathbf{p}^*) - \widetilde{\mathbf{U}}] = \mathbf{0}, \tag{39}$$

where $\mathbf{J}(\mathbf{p})$ is an $(M \times q) \times N$ referred to the *sensitivity matrix* which is given by

$$\mathbf{J}(\mathbf{p}) = \begin{pmatrix} \mathbf{J}_1(\mathbf{p}) \\ \mathbf{J}_2(\mathbf{p}) \\ \vdots \\ \mathbf{J}_q(\mathbf{p}) \end{pmatrix}, \quad \mathbf{J}_k(\mathbf{p}) = \begin{pmatrix} \frac{\partial U_{\ell_1}^{t_k}(\mathbf{p})}{\partial p_1} & \frac{\partial U_{\ell_1}^{t_k}(\mathbf{p})}{\partial p_2} & \cdots & \frac{\partial U_{\ell_1}^{t_k}(\mathbf{p})}{\partial p_N} \\ \frac{\partial U_{\ell_2}^{t_k}(\mathbf{p})}{\partial p_1} & \frac{\partial U_{\ell_2}^{t_k}(\mathbf{p})}{\partial p_2} & \cdots & \frac{\partial U_{\ell_2}^{t_k}(\mathbf{p})}{\partial p_N} \\ \vdots & \vdots & \vdots & \vdots \\ \frac{\partial U_{\ell_M}^{t_k}(\mathbf{p})}{\partial p_1} & \frac{\partial U_{\ell_M}^{t_k}(\mathbf{p})}{\partial p_2} & \cdots & \frac{\partial U_{\ell_M}^{t_k}(\mathbf{p})}{\partial p_N} \end{pmatrix}, \quad k = 1, \ldots, q. \tag{40}$$

Thus, an estimate $\mathbf{p}_\delta$ can be obtained by approximately minimizing the non linear problem (37) such that $\|\mathbf{J}(\mathbf{p}_\delta)^T(\mathbf{U}(\mathbf{p}_\delta) - \widetilde{\mathbf{U}})\|_2$ is small. The minimization problem then requires an iterative method wherein the matrix $\mathbf{J}(\mathbf{p})$ changes at each iteration, and an accurate method for its calculation is necessary. The description of such a method is presented below.

3.1 Sensitivity matrix

Taking partial derivative with respect to p_j on both sides of (23) gives

$$\frac{\partial}{\partial p_j}\mathsf{U}'(t) = \mathsf{A}(\mathbf{p})\frac{\partial \mathsf{U}(\mathbf{p}, t)}{\partial p_j} + \frac{\partial \mathsf{A}(\mathbf{p})}{\partial p_j}\mathsf{U}(\mathbf{p}, t)$$

Letting $\mathsf{V}(\mathbf{p})(t) = \dfrac{\partial \mathsf{U}(\mathbf{p}, t)}{\partial p_j}$, we can interchange the order of differentiation to obtain a system of ODEs with $\mathsf{V}(t)$ as unknown. On the other hand, if (23) is solved for $\mathsf{U}(t)$ it follows that $\dfrac{\partial \mathsf{U}(\mathbf{p}, t)}{\partial p_j}_{|_{t=0}} = 0$. Hence, to determine the jth column of the sensitivity matrix we first solve the initial value problem

$$\begin{cases} \mathsf{V}'(t) = \mathsf{A}(\mathbf{p})\mathsf{V}(t) + \mathsf{W}(t), \quad t > 0, \quad \mathsf{W}(t) = \dfrac{\partial \mathsf{A}(\mathbf{p})}{\partial p_j}\mathsf{U}(\mathbf{p}, \mathsf{t}) \\ \mathsf{V}(0) = 0, \end{cases} . \tag{41}$$

and then take the components of $\mathsf{V}(t)$ corresponding to the locations l_i, $i = 1, \ldots, M$. Notice that this requires solving the direct problem (23) for $\mathsf{U}(\mathbf{p}, t)$.

As already mentioned, in this paper we assume that the direct problem (1)-(6) is solved by using the pseudospectral collocation method, as described in the previous section, and thus, for chosen $\mathbf{p}$ containing approximate values of $P_f(x, y)$ on the grid, $\mathbf{p}(x, y)$, this gives rise to a system matrix given by

$$\mathsf{A}(\mathbf{p}) = \left[(I_n \otimes D_1 D_2) + (B\overline{d}_0 e_1^T + \overline{D}_1\overline{D}_2) \otimes I_{(n+1)} - \overline{\mathsf{P}}_f\right], \tag{42}$$

where $\overline{\mathsf{P}}_f$ is a diagonal matrix given by

$$\overline{\mathsf{P}}_f = \operatorname{diag}\left(\mathbf{p}(x_0, y_0), \ldots, \mathbf{p}(x_n, y_0), \ldots, \mathbf{p}(x_0, y_{n-1}), \ldots, \mathbf{p}(x_n, y_{n-1})\right), \tag{43}$$

thereby indicating that the vector of unknown parameters is

$$\mathbf{p}_f = [P_f(x_0, y_0), \ldots, P_f(x_n, y_0), \ldots, P_f(x_0, y_{n-1}), \ldots, P_f(x_n, y_{n-1})]^T. \tag{44}$$

Notice that by virtue of (42)-(43), the source term of the auxiliary initial value problem (41) reduces to

$$\mathsf{W}(t) = \mathsf{u}_j(\mathbf{p}, t)e_j, \tag{45}$$

where $\mathsf{u}_j(\mathbf{p}, t)$ is the jth component of $\mathsf{U}(\mathbf{p}, t)$ and e_j denotes the jth canonical vector in $\mathbb{R}^{(n+1)n}$.

Having computed efficiently the sensitivity matrix, the nonlinear problem (37) can be handled in several ways. For example by using non linear conjugate gradients (NCG), Gauss-Newton methods, Tikhonov regularization, or others. For an account of a variety of methods for heat inverse problems, the reader is referred to [32].

3.2 Regularized Gauss-Newton method

Linearization of estimated temperatures $\mathbf{U}(\mathbf{p})$ around a current estimate $\mathbf{p}_\delta^k$ at iteration k produces a linear model of the form

$$\widehat{\mathbf{U}}(\mathbf{p}) = \mathbf{U}(\mathbf{p}_\delta^k) + \mathbf{J}^k(\mathbf{p} - \mathbf{p}_\delta^k) \tag{46}$$

where $\mathbf{J}^k$ is introduced to denote $\mathbf{J}^k(\mathbf{p}_\delta^k)$. The Gauss-Newton method for minimizing (37) substitutes this approximation into (39), and defines a sequence of iterative approximations $\mathbf{p}_\delta^k$ given as

$$\mathbf{p}_\delta^{k+1} = \mathbf{p}_\delta^k + \mathbf{s}, \tag{47}$$

where $\mathbf{s}$ solves the linear least squares problem

$$\min_{\mathbf{s}} \|\mathbf{U}(\mathbf{p}_\delta^k) - \widetilde{\mathbf{U}} + \mathbf{J}^k(\mathbf{p} - \mathbf{p}_\delta^k)\|_2^2. \tag{48}$$

Alternatively, provided $(\mathbf{J}^k)^T(\mathbf{J}^k)$ is non singular, the sequence of iterative approximations is given as

$$\mathbf{p}_\delta^{k+1} = \mathbf{p}_\delta^k - [(\mathbf{J}^k)^T(\mathbf{J}^k)]^{-1}(\mathbf{J}^k)^T[\mathbf{U}(\mathbf{p}_\delta^k) - \widetilde{\mathbf{U}}],\ k = 0, 1, \ldots \tag{49}$$

In inverse heat transfer problems the sensitivity matrix $\mathbf{J}^k$ is usually very ill-conditioned, so that the iterative approximations $\mathbf{p}_\delta^k$ will be unstable even if $[(\mathbf{J}^k)^T(\mathbf{J}^k)]$ is nonsingular. The regularized Gauss-Newton method alleviates such difficulty by adding a stabilization term to (48) so that the iterative approximations are obtained by solving the least squares problem

$$\min_{\mathbf{s}} \|[\mathbf{U}(\mathbf{p}_\delta^k) - \widetilde{\mathbf{U}}] + \mathbf{J}^k(\mathbf{p} - \mathbf{p}_\delta^k)\|_2^2 + \lambda_k^2\|\mathbf{L}(\mathbf{p} - \mathbf{p}_e)\|_2^2, \tag{50}$$

where $\mathbf{L}$ is a regularization matrix introduced to damp instabilities, λ_k is a monotonically decreasing sequence of regularization parameters satisfying [14, 16]

$$\lambda_k > 0, \quad 1 \leq \frac{\lambda_k}{\lambda_{k+1}} \leq C, \quad (C = \text{const.}), \tag{51}$$

and $\mathbf{p}_e$ is an a priori estimate of $\mathbf{p}_f$. The regularization matrix is generally chosen to be either the identity matrix or some discrete differential operator.

Under the mild condition that $\mathcal{N}(\mathbf{J}^k) \cap \mathcal{N}(\mathbf{L}) = \{0\}$, where $\mathcal{N}(\cdot)$ stands for null space of $(\cdot)$, using the regularized normal equations associated to (50) it follows that the iterative approximations satisfy

$$\mathbf{p}_\delta^{k+1} = \mathbf{p}_\delta^k - [(\mathbf{J}^k)^T(\mathbf{J}^k) + \lambda_k^2\mathbf{L}^T\mathbf{L}]^{-1}\left\{(\mathbf{J}^k)^T[\mathbf{U}(\mathbf{p}_\delta^k) - \widetilde{\mathbf{U}}] + \lambda_k^2\mathbf{L}^T\mathbf{L}(\mathbf{p}_\delta^k - \mathbf{p}_e)\right\} \tag{52}$$

Several strategies for selecting regularization parameter satisfying (51) can be considered among a number of regularization methods for linear problems such as Generalized Cross-validation, L-curve, discrepancy principle, Reginska's rule, Fixed-point method (FP), etc [2, 3, 21]. However, as mentioned in [14], numerical experiments have shown that a brutal use of the above parameter choice methods may lead to oscillating sequences λ_k [14]. A way to alleviate this difficulty was proposed by Eriksson [16] who suggested a sequence of regularization parameters defined by :

$$\lambda_k = \begin{cases} \xi\lambda_{k-1} + (1-\xi)\lambda, & \lambda < \lambda_{k-1}, \\ \lambda_{k-1}, & \lambda \geq \lambda_{k-1}, \end{cases} \tag{53}$$

where λ is the regularization parameter determined by one of the above methods and $0 < \xi < 1$ is chosen a priori. An important aspect concerning the construction of stable approximation via iterative methods is the choice of the stopping index. More precisely, for iterative regularization methods, the number of iteration steps plays the role of the regularization parameter, and thus the iterations have to be properly stopped in order to keep the contribution of noise in the approximations under control. A widely used rule for selecting the stopping index is the discrepancy principle (DP), that is, the iterative process is stopped at the first index $\breve{k} = \breve{k}(\delta)$ such that

$$\|[\mathbf{U}(\mathbf{p}_\delta^{\breve{k}}) - \widetilde{\mathbf{U}}\| \leq \tau_d\delta < \|[\mathbf{U}(\mathbf{p}_\delta^k) - \widetilde{\mathbf{U}}]\|_2, \quad 0 \leq k \leq \breve{k} \tag{54}$$

where $\tau_d > 1$ and δ satisfying (38). Unfortunately, because in many inverse heat transfer problems the errors in the data cannot be estimated, alternative ways to stop the iterative process which do not rely on a priori knowledge of the error norm are necessary.

Assuming that the error norm estimate δ is not available, the proposal of this work is to compute iterative approximations for the perfusion coefficient P_f obtained by the regularized Gauss-Newton method using the Fixed-point method as parameter choice rule. The proposal relies on the observation that, because computed temperatures U associated to the bioheat problem vary very slowly with time, the singular values of the sensitivity matrix $\mathbf{J}^k$ do not vary significantly during the iteration process. Based on this observation and on the excellent performance of the Fixed-point method compared to L-curve method in solving linear problems, see examples in [2, 3, 4, 5], for the sequence of regularization parameters (51) we choose a sequence λ_k as defined in (53) in which the regularization parameter λ is determined by the Fixed-point method. In addition, in order to guarantee that λ_k is actually decreasing, if $\lambda > \lambda_{k-1}$ we take $\lambda_k = \varsigma\lambda_{k-1}$ for $\varsigma \lessapprox 1$. This regularization parameter choice method will be referred to as the weighted FP-method.

For purposes of clarity, the Fixed-point method will be described briefly. For $\lambda > 0$ let $\mathbf{p}_\lambda^k$ be the regularized solution to the minimization problem (50) with λ instead of λ_k. The regularization parameter chosen by the Fixed-point method associated to this linear problem is a limit value of the sequence defined by

$$\lambda^{(j+1)} = \Phi^{(k)}(\lambda^{(j)}), \quad \Phi^{(k)}(\lambda) = \frac{\|[\mathbf{U}(\mathbf{p}_\delta^k) - \widetilde{\mathbf{U}}] + \mathbf{J}^k(\mathbf{p}_\lambda^{(k)} - \mathbf{p}_\delta^k)\|_2}{\|\mathbf{L}\mathbf{p}_\lambda^{(k)}\|_2}, \; j = 0, 1, \ldots. \tag{55}$$

That is, the regularization parameter computed this way is a fixed-point of $\Phi^{(k)}$. Theoretically, this parameter minimizes the product of the residual norm (the numerator of $\Phi^{(k)}(\lambda)$) and the seminorm $\|\mathbf{L}\mathbf{p}_\lambda^{(k)}\|$, and corresponds to a good balance between the size of these norms. Interestingly enough, the Fixed-point method does not require any a priori knowledge of the error norm. Furthermore, it can be computed efficiently using the generalized singular value decomposition (GSVD) of the matrix pair $(\mathbf{J}^k, \mathbf{L})$. For algorithmic details of the Fixed-point method and stopping criterion the reader is referred to [2, 3].

As stopping criterion for the regularized Gauss-Newton method, we choose to stop the iterations as soon as the relative change in λ_k reaches some prescribed tolerance. The motivation

for this stopping rule relies on the fact that computed temperature values associated to the bioheat problem change very slowly, in which case the function $\Phi^{(k)}(\lambda)$ varies slowly with k during the iterative process. As a result, the sequence of regularization parameters λ_k turns out to stagnate very quickly, as we will illustrate numerically later. This gives rise to an algorithm which we denote by RGN-FP and summarize as follows.

Regularized Gauss-Newton method with FP as parameter choice rule:

Input data : Tol, n, regularization matrix $\mathbf{L}$, a priori estimate $\mathbf{p}_e$, initial guess $\mathbf{p}_\delta^0$, measured temperatures $\widetilde{\mathbf{U}}$.

Set $k = 0$, $\lambda_{-1} = 0$

1. Set $\mathbf{p} = \mathbf{p}_\delta^k$ and solve both the forward problem (35) and the initial value problem (41) to obtain $\mathbf{U}(\mathbf{p}_\delta^k)$ and the sensitivity matrix J^k.
2. Using the GSVD of the matrix pair $(\mathbf{J}^k, \mathbf{L})$ determine the fixed point λ of $\Phi^{(k)}$, as described in (55), and compute λ_k according to the weighted FP-method.
3. Compute the new estimate $\mathbf{p}_\delta^{(k+1)}$ by solving the least squares problem (50)
4. Compute the ratio $\rho_k = |\lambda_k - \lambda_{k-1}|/\lambda_k$.
   If $\rho_k < Tol$
   Stop the iterations and take $\mathbf{p}_f = \mathbf{p}_\delta^{k+1}$.
   Otherwise
   set $k \leftarrow k + 1$ and go to step 1.

We close this section with an observation regarding a comparison of the stopping index determined by RGN-FP compared to the one determined by the discrepancy principle DP. For this, notice that the residual corresponding to the regularized solution $\mathbf{p}_\lambda^k$ to the least squares problem (50) (actually Tikhonov problem) is given as $r_\lambda^k = [\mathbf{U}(\mathbf{p}_\delta^k) - \widetilde{\mathbf{U}}] + \mathbf{J}^k(\mathbf{p}_\lambda^{(k)} - \mathbf{p}_\delta^k)$. Hence, if at step k we determine the fixed point of $\Phi^{(k)}$, say $\lambda^* = \Phi^{(k)}(\lambda^*)$, then we have $\lambda_k = \lambda^*$ and hence, $\mathbf{p}_\lambda^* = \mathbf{p}_\delta^{k+1}$. Therefore at step k we have

$$\|r_{\lambda^*}^k\|_2 = \|[\mathbf{U}(\mathbf{p}_\delta^k) - \widetilde{\mathbf{U}}] + \mathbf{J}^k(\mathbf{p}_\delta^{k+1} - \mathbf{p}_\delta^k)\| \leq \|[\mathbf{U}(\mathbf{p}_\delta^k) - \widetilde{\mathbf{U}}]\|_2 + \|\mathbf{J}^k\|_2 \|\mathbf{p}_\delta^{k+1} - \mathbf{p}_\delta^k\|_2.$$

Hence, if the tolerance criterion at step 4 of RGN-FP is satisfied at $k = k^*$, then the sequence of regularization parameters λ_k stagnates, and as a result we have $\mathbf{p}_\delta^{k+1} \approx -\mathbf{p}_\delta^k$, and the related residual norm can be bounded as

$$\|r_{\lambda^*}^{k^*}\|_2 \lessapprox \|[\mathbf{U}(\mathbf{p}_\delta^{k^*}) - \widetilde{\mathbf{U}}]\|_2$$

Thus, since in general the tolerance criterion at step 4 of RGN-FP is satisfied in a few iterations, the estimate above suggests that RGN-FP should stop in less steps than the discrepancy principle does.

4 Numerical Examples

This section illustrates numerically the effectiveness of RGN-FP on several test problems involving 1D and 2D cases. We first consider the case where P_f depends on x, which covers a number of cases discussed in literature [29, 42], and then the case where P_f depends on both spatial variables. In both cases, to simulate measured temperature values we first assume that sensors are located at even-numbered grid points of 9 successive central rows of the grid, where the numbering of gridpoints is as in Fig. 2, and consider temperature values $U_{\ell_i}^{t_k}$ at eight time levels $t_k = 200\,k\Delta t$, $k = 1, \ldots, 8$, where Δt is the maximum allowable timestep for stable integration of (35). If, $n = 14$, for instance, this gives 63 measurement locations, the number

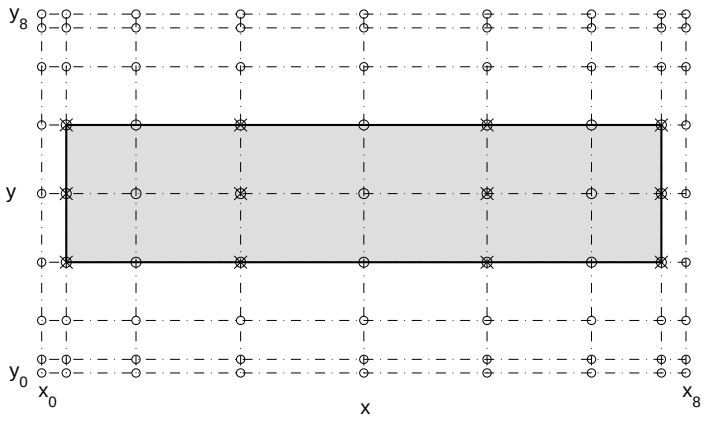

Figure 7: Grid points (marked with small circle) and sensor locations (marked with × symbol).

of unknown parameters for 1D estimation is $m = n + 1$, $\Delta t = 1.8 \times 10^{-4}$ for **CPS-RK4** and the sensitivity matrix $\mathbf{J}^k$ is 504×15. The measurement procedure is illustrated in Fig. 7, grey region, where we consider three central rows and $n = 8$. Then, arranging all exact temperature values $U_{\ell_i}^{t_k}$ in a long vector $\mathbf{U}$, we simulate actual measured temperature data as

$$\widetilde{\mathbf{U}} = \mathbf{U} + \mathbf{n},$$

where $\mathbf{n}$ is a Gaussian random vector generated by the Matlab function randn with the state value set to zero, and $\mathrm{NL} = \|\mathbf{n}\|_2/\|\mathbf{U}\|_2$ is referred to as the *noise level* in the data. For each test problem the measurement process is repeated for 30 different random sequences and for each data set generated in this way we estimate the corresponding perfusion coefficient and then compute average values of the estimation error for several noise levels.

For the implementation of RGN-FP for the 1D case we use **CPS-RK4** as forward solver. Input parameters are chosen as

$$Tol = 0.0001, \quad \mathbf{p}_e = \mathbf{p}_\delta^0 = 0, \tag{56}$$

and the regularization matrix is defined by

$$\mathbf{L}_1(m) = \begin{bmatrix} -1 & 1 & & \\ & \ddots & \ddots & \\ & & -1 & 1 \end{bmatrix} \in \mathbb{R}^{(m-1)\times m}, \tag{57}$$

where m denotes the number of unknown parameters. Computation were carried out in Matlab.

4.1 1D estimation

For the numerical examples involving the 1D case the source term $G(x, y, t)$ is chosen in such a way that the solution to the bioheat problem (1)-(6) for given perfusion coefficient P_f is the function $U(x, y, t)$ defined in (25). Two types of perfusion coefficient are selected: two test cases involving smooth P_fs and an third one involving a nonsmooth P_f.

Smooth P_f

We consider two examples:

(a) $P_f(x) = x^2$,
(b) $P_f(x) = 5\left[2 + \cos(x\pi) - \cos(2x\pi) - \cos(3x\pi) - \cos(4x\pi)\right]$.

For case (a) (relatively easy), we choose $n = 14$ and consider five noise levels: NL $= 10^{-6}, 10^{-5}$, $10^{-4}, 10^{-3}, 10^{-2}$ and 10^{-1}, which means the data are corrupted with noise levels 0.0001%, 0.001%, 0.01% 0.1% and 1%, respectively. The very low noise level case is introduced to illustrate the behavior of the estimated parameter as the noise level goes to zero.

Average relative estimation errors of 30 realizations for several noise levels are displayed in Fig 8. We notice that the quality of the estimated coefficient deteriorates as the noise level increases, but we notice also that the quality is excellent for the lowest noise level.

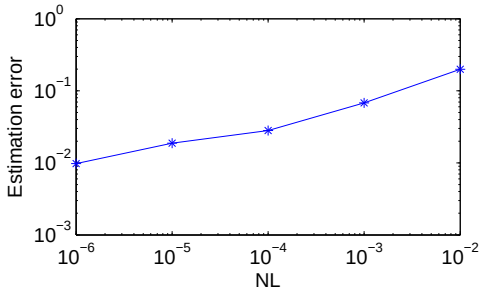

Figure 8: Average values of estimation errors for P_f of example (a) for five noise levels.

Condition numbers of $\mathbf{J}^k$ and fixed points of $\Phi^{(k)}$ as functions of the number of iterations for a typical run are displayed in Fig. 9. Fast stagnation of both the condition number of $\mathbf{J}^k$ and the fixed points of $\Phi^{(k)}$ suggests that RGN-FP should converge in a few iterations. As a matter of fact, for the run considered in Figure 9 RGN-FP stopped at $k = 7$.

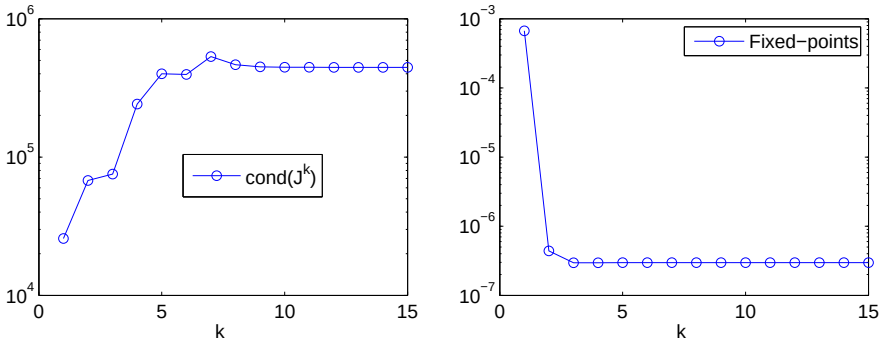

Figure 9: Conditioning of sensitivity matrix $\mathbf{J}^k$ and fixed-points of $\Phi^{(k)}$ for example 1-(a) using data with relative noise level NL $= 10^{-4}$%.

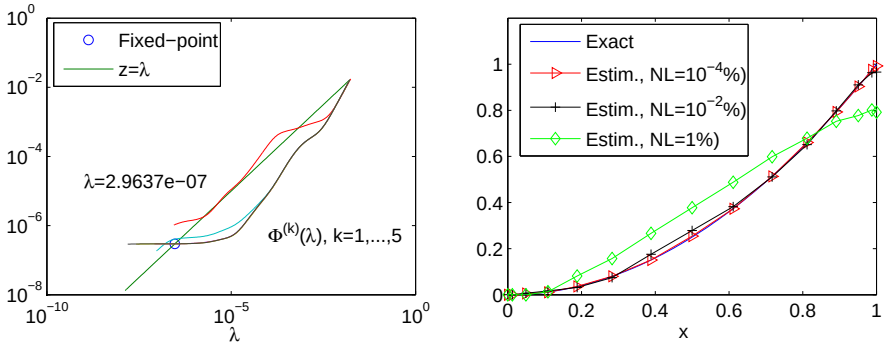

Figure 10: Behavior of function $\Phi^{(k)}$ for NL $= 10^{-4}$ % (left) and estimated coefficients (right)

Figure 10 shows the typical behavior of functions $\Phi^{(k)}$ for $k = 1, 2, \ldots 5$ for the smallest noise level and typical results of the estimation process for three noise levels.

Case (b) is not as easy as case (a) since the exact perfusion coefficient P_f exhibits some oscillations that are somewhat difficult to resolve. In order to compensate this difficulty we increase the number of grid points (hence the number of locations) to $n = 20$. This gives 90 measurement locations and yields a sensitivity matrix $\mathbf{J}^k$ of size 720×21. As in the previous example, we compute average relative estimation errors of 30 realizations which are displayed in Fig. 11. Notice that the estimation errors for case (b) follow the same trend as those of case (a).

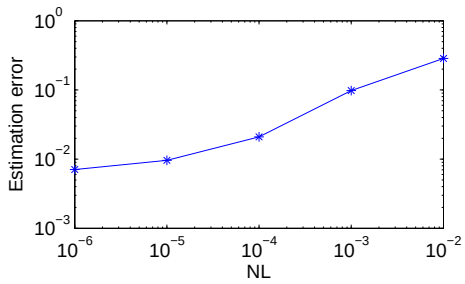

Figure 11: Average values of estimation errors for P_f of example (b) for five noise levels.

Figure 12 shows the behavior of fixed points of $\Phi^{(k)}$ as a function of the iteration index k and some of the corresponding functions. Again, since the sequence of fixed points stagnates very quickly, the stopping criterion of RGN-FP is satisfied early. Typical estimated coefficients for $NL = 10^{-6}$ and $NL = 10^{-2}$ (with stopping index $k^* = 8$ and $k^* = 6$, respectively, are displayed in Figure 13.

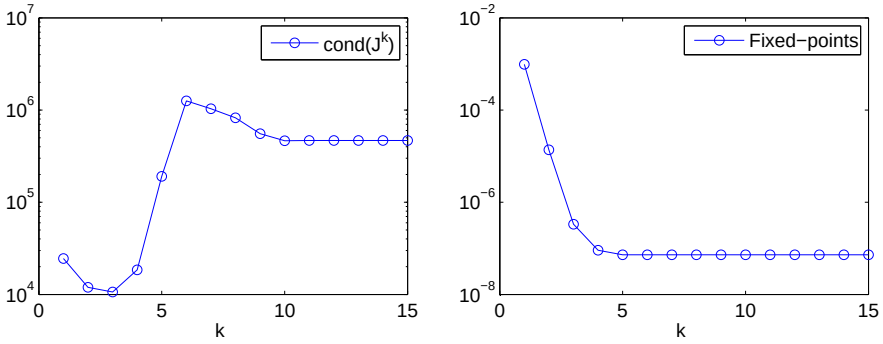

Figure 12: Conditioning of sensitivity matrix J^k and fixed-points of $\Phi^{(k)}$ for example 1-(b) using noisy data with relative noise level NL $= 10^{-6}$.

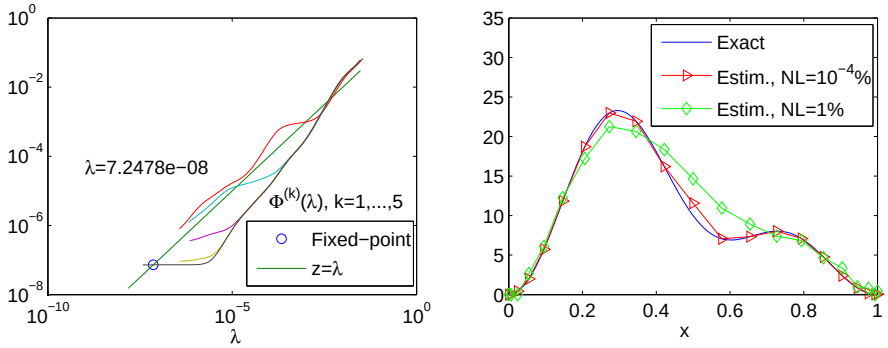

Figure 13: Behavior of function $\Phi^{(k)}$ for NL $= 10^{-4}$ % (left) and estimated coefficients (right).

Nonsmooth P_f

We consider the estimation problem for the case when the perfusion coefficient is not differentiable on all domain. Our test problem involves the perfusion coefficient given in (33). As estimation problems involving nonsmooth coefficient are know to be very difficult, we will compensate the difficulties associated to this kind of problems by increasing the number of grid-points to $n = 22$. We then, as before, consider five noise levels and proceed as in the previous examples. The behavior of fixed-points and results of the estimation procedure of typical runs for two noise levels are displayed in Figure 14. The difficulties associated to the nonsmooth case are eloquent from the results: acceptable reconstructions are only possible for very low noise level cases. Similar conclusions concerning this test problem can be found in [29]. The estimated parameters were obtained with $k^* = 12$ for the very low noise level case and $k^* = 8$ for the other case. The quality of average relative estimation errors decrease a little if compared with the previous examples but the trend is approximately the same; this explains why these results are not displayed here.

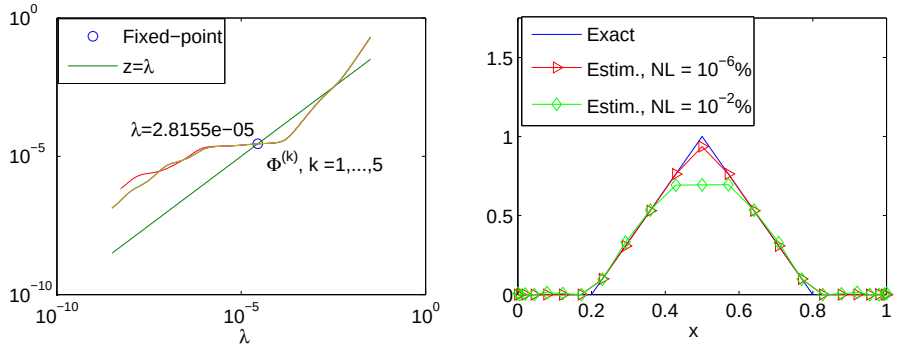

Figure 14: Functions $\Phi^{(k)}$ (left) and results for nonsmooth P_f case using noisy data. Functions on the left correspond to noise level NL $= 10^{-4}$.

4.2 2D estimation

This section is concerned with a perfusion estimation problem where P_f depends on both spatial variables. The purpose is to test our RGN-FP algorithm coupled with **CPS-RK2** and **CPS-RK4** as forward solvers. For this, we consider a bioheat problem whose source term is defined by

$$G(x, y, t) = -e^{-\pi^2 t}\cos(\pi x) + P_f(x, y)U(x, y, t),$$

with perfusion coefficient defined by $P_f(x, y) = \sin(\pi xy)$, and exact solution

$$U(x, y, t) = \frac{e^{-\pi^2 t}}{2(B + L)}[((B + L)y^2 - By - L)\cos(\pi x)] + \frac{BU_\infty}{B + L}(L - y). \tag{58}$$

For the numerical simulation we choose $B = 0.015,\ U_\infty = 0.001,\ L = 1$, and initial temperature value $U_0 = \dfrac{1}{2(B + 1)}[((B + 1)y^2 - By - 1)\cos(\pi x)] + \dfrac{BU_\infty}{B + 1}(1 - y)$.

Notice that this 2D perfusion coefficient estimation problem involves $(n+1) \times n$ unknowns, as seen from vector $\mathbf{p}_f$ in (44). So in order to keep the number of unknowns within reasonable bounds we choose $n = 14$ (which means we deal with an optimization problem involving 210 unknowns). For the simulation of the measurement process we follow the same protocol as in the previous examples. Thus, we consider 63 measurements locations and 8 time levels, in which case the sensitivity matrix $\mathbf{J}^k$ is of order 504×210. In order to stabilize the RGN iterations

we consider three cases for the regularization matrix. In the first case $\mathbf{L}$ is the identity matrix, and in the second and third cases $\mathbf{L}$ is a 2D discrete differentiation operator of the form

$$\mathcal{L}_i = \begin{bmatrix} I_n \otimes \mathbf{L}_i(n+1) \\ \mathbf{L}_i(n) \otimes I_{n+1} \end{bmatrix}, \; i = 1, 2,$$

where $\mathbf{L}_1(m)$ is defined in (57) and $\mathbf{L}_2(m)$ is a 1D second order discrete differentiation operator defined by

$$\mathbf{L}_2(m) = \begin{bmatrix} 1 & -2 & 1 & & & \\ & 1 & -2 & 1 & & \\ & & \ddots & \ddots & \ddots & \\ & & & 1 & -2 & 1 \end{bmatrix} \in \mathbb{R}^{(m-2)\times m}. \tag{59}$$

Regularizers $\mathcal{L}_i$ are often employed in image reconstruction problems [5]; the purpose of them is to incorporate in the iterative process smoothing properties of P_f in the horizontal and vertical directions. The purpose of the three choices of $\mathbf{L}$ is to provide the reader with further insight concerning the role that the regularizer plays into the stabilization of the inverse problem.

We first describe results obtained with RGN-FP coupled with **CPS-RK2** using perturbed data with NL = 0.01% and start by showing that the all chosen regularization are able to stabilize RGN. This is illustrated in Figure 15 in which, condition numbers J^k and fixed points of Φ^k are displayed. Notice that stagnation of these quantiles occur very early. In this case, the stopping criterion of RGN-FP is reached in 9 iteration for $\mathbf{L} = I$ and in 8 iterations for $\mathbf{L} = \mathcal{L}_2$.

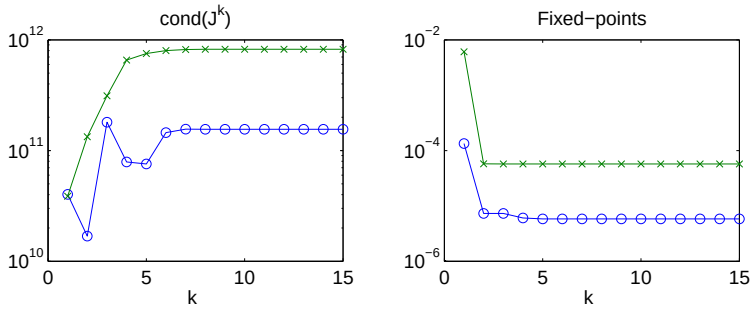

Figure 15: Condition numbers of J^k and fixed-points of Φ^k. Small circles correspond to $\mathbf{L} = I$ and x marks correspond to $\mathbf{L} = \mathcal{L}_2$. Quantities corresponding to $\mathbf{L} = \mathcal{L}_1$ behaved similarly and are not displayed here.

The results of the estimation process are shown in Figure 16, using a 3D graph (first row) to visualize $P_f(x, y)$ over the grid points, as well as using a 2D graph (second row) to display the parameter vector $\mathbf{p}_f$ and its estimates $\mathbf{p}_\delta^k$. This test problem provides an excellent way to illustrate the fact that stabilization of RGN may not be sufficient to guarantee good solutions, as seen from the results corresponding to $\mathbf{L} = I$.

In order to illustrate the quality of the results obtained using both **CPS-RK2** and **CPS-RK4** as forward solvers, we compute the actual error $\mathbf{p}_f - \mathbf{p}_\delta^k$ where $\mathbf{p}_\delta^k$ denotes the estimated parameter obtained in each case. The conclusion drawn in this case is that the quality produced by both solvers is essentially the same, as displayed in Fig. 17 (left). Finally, in order to illustrate the effect of the noise level on the quality of the results, we also use data with noise level NL = 1%. In this case, for clarity, the results are presented through a 2D graph in Fig. 17 (right) which also includes results corresponding to the low noise level; in both cases only results obtained using **CPS-RK2** are displayed. As before, we notice that the quality of the estimated parameter for the smallest noise level is excellent, and that this quality deteriorates as the noise

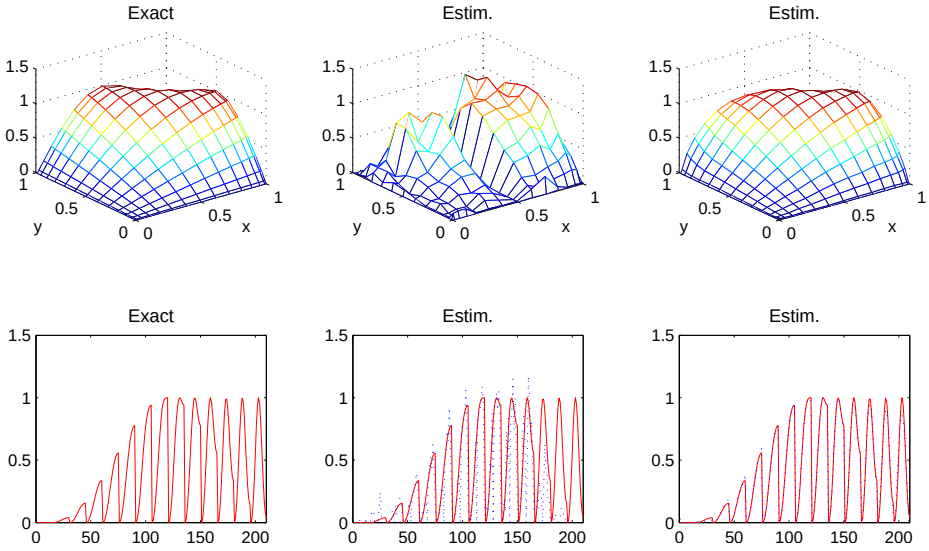

Figure 16: Exact and estimated perfusion coefficients: Results corresponding to $\mathbf{L} = I$ (second column) and results corresponding to $\mathbf{L} = \mathcal{L}_2$ (third column). Quantities corresponding to $\mathbf{L} = \mathcal{L}_1$ behaved similarly as those obtained with $\mathbf{L} = \mathcal{L}_2$ and are not displayed here.

level grows. Finally, we emphasize that, similar to the 1D cases, we also computed average relative estimation errors. The behavior of these reconstruction errors behaved very similarly as the 1D cases and are therefore not displayed here.

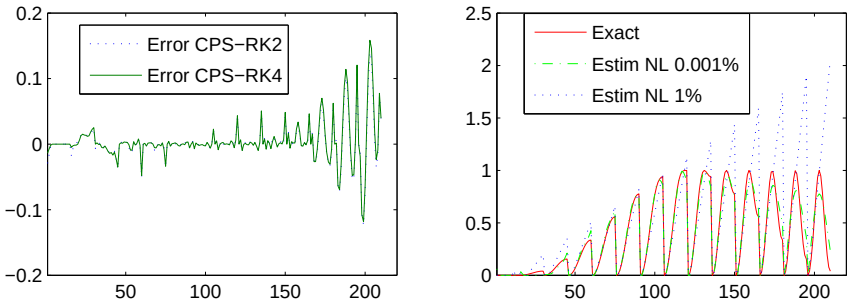

Figure 17: Error for noise level NL $= 10^{-2}$ % (left). Exact parameter $\mathbf{p}_f$ and estimated parameters $\mathbf{p}^k$ (right).

5 Conclusions

We investigated the problem of estimating the perfusion coefficient as a function of position from a 2D heat transfer Pennes model. As a result, we proposed a parameter estimation method based on both a highly accurate approach for the forward problem, and the regularized Gauss-Newton method to cope with typical instabilities in inverse estimation problems. Numerical results using synthetic data not only show that the proposed method is effective but also that it may be useful in practical applications such as therapeutic procedures by hyperthermia or other procedures depending on blood perfusion measurements. Continued experience with the proposed protocol is necessary to fully assess its potential. In particular, the influence of sensor locations (and number) on the quality of the perfused coefficient should be investigated. More experience is needed with problems involving real data. Moreover, extension of the proposed protocol to the case when the perfusion coefficient also depends on time is highly desirable. These are the subject of future research.

Acknowledgements

The authors are gratefult to the reviewers by suggestions/comments that improved the presentation of this work.

References

[1] H. G. Bagaria, D. T. Johnson, Transient solution to the bioheat equation and optimization for magnetic fluid hyperthermia treatment, Int. J. of Hyperthermia, 21 (2005) 57–75.

[2] F.S.V. Bazán, Fixed-point iterations in determining the Tikhonov regularization parameter, Inverse Problems 24 (2008) 1–15.

[3] F.S.V. Bazán, J.B. Francisco, An improved Fixed-point algorithm for determining a Tikhonov regularization parameter, Inverse Problems 25 (2009) 045007 .

[4] F.S.V. Bazán, L.S. Borges, GKB-FP: an algorithm for large-scale discrete ill-posed problems, BIT (2010) DOI 10.1007/s10543-010-0275-3 .

[5] F.S.V. Bazán, M.C.C. Cunha, L.S. Borges, Extension of GKB-FP algorithm to large-scale general-form Tikhonov regularization, Numer. Lin. Alg., (0213) DOI: 10.1002/nla.1874.

[6] A. Belmiloudi, Parameter identification problems and analysis of the impact of porous media in biofluid heat transfer in biological tissues during thermal therapy, Nonlinear Analysis: Real World Applications, 11 (2010) 1345–1363.

[7] L. Bedin, F.S.V. Bazán, A note on existence and uniqueness of solutions for a 2D bioheat problem, Applicable Analysis, DOI: 10.1080/00036811.2016.1148138, Feb. 2016.

[8] L. Bedin and F.S.V. Bazán, On the 2D bioheat equation with convective boundary conditions and its numerical realization via a highly accurate approach, Applied Mathematics and Computation v. 236, p. 422-436, 2014.

[9] F.S.V. Bazán, L. Bedin, F. Bozzoli, Numerical estimation of convective heat transfer coefficient through linearization, Int. J. Heat Mass Transfer 102 (2016) 1230-1244.

[10] S. Canuto, M. Y. Hussaini, A. Quarteroni, and T. A. Zang, Spectral Methods. Fundamentals in Single Domains, Springer, Heidelberg, 2006.

[11] M. J. Colaço, H. B. Orlande, G. S. Dulikravich, Inverse and optimization problems in heat transfer, J. of the Braz. Soc. of Mech. Sci. & Eng. XXVIII(1) (2006) 1–24.

[12] Z. Deng, J. Liu, Mathematical modeling of temperature mapping over skin surface and its implementation in thermal disease diagnostics, Computers in Biology and Medicine 34 (2004) 495–521.

[13] M. Deghan, M. Sabouri, A spectral element method for solving the Pennes bioheat transfer equation by using triangular and quadrilateral elements, App. Math. Modelling 36 (2012) 6031–6049.

[14] A. Doicu, F. Schreier, M. Hess, Iteratively regularized Gauss-Newton method for atmospheric remote sensing, Comput. Phys. Commun. 148 (2002) 214-26.

[15] T. Drizdal, P. Togni, L. Visek, J. Vrba, Comparison of Constant and Temperature Dependent Blood Perfusion in Temperature Prediction for Superficial Hyperthermia, Radioengineering, 19(2) (2010) 281-289.

[16] J. Eriksson, Optimization and regularization of nonlinear least squares problems, Ph.D thesis, Department of Computing Science, Umeä University, Sweden, 1996.

[17] J. Fan, L. Wang, Analytical theory of bioheat transport, J. Appl. Phys. 109 (2011) 1–43.

[18] B. Fornberg, A Practical Guide to Pseudospectral Methods, Cambridge University Press, Cambridge, 1996.

[19] J. B. Francisco and F. S. V. Bazán. Nonmonotone algorithm for minimization on closed sets with application to minimization on Stiffen manifolds. Journal of Computational and Applied Mathematics, 236(10):2717–2727, 2012.

[20] M. Giordano, G. Gutierrez, C. Rinaldi, Fundamental solutions to the bioheat equation and their application to magnetic fluid hyperthermia, Int. J. Hyperthermia, 26(5) (2006) 475-484.

[21] P.C. Hansen, Rank-Deficient and Discrete Ill-Posed Problems, SIAM, Philadelphia, 1998.

[22] J. Iljaž, L. Škerget, Blood perfusion estimation in heterogeneous tissue using BEM based algorithm, Engineering Analysis with Boundary Elements 39, 75-87, 2014.

[23] F. Incropera, D.P. De Witt, T. L. Bergman, A. S. Lavine, Fundamentals of Heat and Mass Transfer, John Wiley & Sons, 2006.

[24] A. Lakhassi, E. Kengne, H. Semmaoui, Modified Penne's equation modelling bioheat transfer in living tissues: analytical and numerical analysis, Natural Sciences, 2(12) (2012) 1375–1385.

[25] H.J. Li, X. Zhang, Y.F. Yi, Measurement of Blood Perfusion Using the Temperature Response to Constant Surface Flux Heating, Int. J. of Thermophysics, 23(6) (2002), 1631-1644.

[26] J. Liu, L. X. Xu, Boundary information based diagnostics on the thermal states of biological bodies, Int. J. Heat and Mass Transfer 43 (2000) 2827-2839.

[27] Z. F. Liu, G. Zhao, Y. H. Cheng, D. Y. Gao, Heating effect of thermally significant blood vessel in perfused tumor tissue during cryosurgery, Journal of Mechanics in Medicine and Biology, 12(1) (2012) 1-16.

[28] J. Liu, L.J. Xu, Estimation of blood perfusion using phase shift in temperature response to sinusoidal heating at the skin surface, IEEE Trans Biomed Eng., 46(9) (1999), 1037–1043.

[29] C. F. L. Souza, M. V. C. Souza, M. J. Colaço, A. B. Caldeira, F. Scofano Neto, Inverse determination of blood perfusion coefficient by using different deterministic and heuristic techniques, J. Braz. Soc. Mech. Sci. Eng. 36(1), 193-206, 2014.

[30] M. Miyakawa, J.C. Bolomey, Non-Invasive Thermometry of the Human Body, CRC Press, 1996.

[31] A.V. Mudaliar, B. Ellis, P. L. Ricketts, O. I. Lanz, C. Y. Lee, T. E. Diller, E. P. Scott, Noninvasive Blood Perfusion Measurements of an Isolated Rat Liver and an Anesthetized Rat Kidney, J. Biomech. Eng., 130(6) (2008) 061013

[32] M. N. Ozisik, H. R. B. Orlande, Inverse heat transfer, Taylor & Francis, New York, 2000.

[33] R.Z. Pei, L. Jing, W.C. Cheng, J. P. Xue, Boundary Element Method (BEM) for Solving Normal and Inverse Bio-Heat Transfer Problem of Biological Bodies with Complex Shape, Journal of Thermal Science 4(2) (1995) 177-184.

[34] H. H. Pennes, Analysis of tissue and arterial blood temperatures in the resting human forearm, J. Appl. Physiology 1(2) (1948) 93–122.

[35] R. Peyret, Spectral Methods for Incompressible Viscous Flow, Springer, Heildelberg, 2002. function method, Int. J. of Appl. Math and Mech. 8(17) (2012) 98–111.

[36] W. Shen, J. Zhang, Modeling and numerical simulation of bioheat transfer and biomechanics in soft tissue, Math. Comput. Model. 41 (2005) 1251–1265.

[37] T. C. Shih, Y. Ping, W. Lin, H. Kou, Analytical analysis of the Pennes bioheat transfer equation with sinusoidal heat flux condition on skin surface, Medical Engineering & Physics 29 (2007) 946–953.

[38] T. C. Sideris, Ordinary Differential Equations and Dynamical Systems, Atlantis Press, Paris, 2013.

[39] Ph. L. Toint, Non-monotone trust region algorithm for nonlinear optimization subject to convex constraints, Mathematical Programming, 77:69–94, 1997.

[40] L. N. Trefethen, Spectral Methods in Matlab, SIAM, Philadelphia, PA, 2000.

[41] D. Trucu, D. B. Ingham, D. Lesnic, Inverse time-dependent perfusion coefficient identification, Journal of Physics: Conf. Series 124 (2008) Paper 012050.

[42] D. Trucu, D. B. Ingham, D. Lesnic, Space-dependent perfusion coefficient identification in the transient bio-heat equation, Journal of Eng. Math. 67 (2010) 307–315.